Electronic Supplementary Information

Molecular Characterization of Ultrafine Particles using Extractive Electrospray Time-of-Flight Mass Spectrometry

Mihnea Surdu[1,*], Veronika Pospisilova[1,a,*], Mao Xiao[1], Mingyi Wang[2], Bernhard Mentler[3], Mario Simon[4], Dominik Stolzenburg[5], Christopher R. Hoyle[1,6], David M. Bell[1], Chuan Ping Lee[1], Houssni Lamkaddam[1], Felipe Lopez-Hilfiker[1], Lauri R. Ahonen[7], Antonio Amorim[8], Andrea Baccarini[1,9], Dexian Chen[2], Lubna Dada[1,7], Jonathan Duplissy[7,10], Henning Finkenzeller[11], Xu-Cheng He[7], Victoria Hofbauer[2], Changhyuk Kim[12,13], Andreas Kürten[4], Aleksandr Kvashnin[15], Katrianne Lehtipalo[7,16], Vladimir Makhmutov[15], Ugo Molteni[1,b], Wei Nie[17], Antti Onnela[14], Tuukka Petäjä[7], Lauriane L.J. Quéléver[7], Christian Tauber[5], António Tomé[18], Robert Wagner[7], Chao Yan[7], Andre S.H. Prevot[1], Josef Dommen[1], Neil M. Donahue[2], Armin Hansel[3], Joachim Curtius[4], Paul M. Winkler[5], Markku Kulmala[7,10], Rainer Volkamer[11], Richard C. Flagan[12], Jasper Kirkby[4,14], Douglas R. Worsnop[7,19], Jay G. Slowik[1], Dongyu S. Wang[1], Urs Baltensperger[1], Imad el Haddad[1]

[1]Laboratory of Atmospheric Chemistry, Paul Scherrer Institute, 5232 Villigen, Switzerland
[2]Center for Atmospheric Particle Studies, Carnegie Mellon University, 15213 Pittsburgh, PA, USA.
[3]Institute of Ion Physics and Applied Physics, University of Innsbruck, 6020 Innsbruck, Austria
[4]Institute for Atmospheric and Environmental Sciences, Goethe University Frankfurt, 60438 Frankfurt am Main, Germany
[5]Faculty of Physics, University of Vienna, 1090 Vienna, Austria
[6]Institute for Atmospheric and Climate Science, ETH Zurich, 8006 Zurich, Switzerland
[7]Institute for Atmospheric and Earth System Research (INAR)/Physics, Faculty of Science, University of Helsinki, 00014 Helsinki, Finland
[8]CENTRA and FCUL, University of Lisbon, 1749-016 Lisbon, Portugal
[9]School of Architecture, Civil and Environmental Engineering, École Polytechnique Fédérale de Lausanne, 1015 Lausanne, Switzerland
[10]Helsinki Institute of Physics, University of Helsinki, 00014 Helsinki, Finland
[11]Department of Chemistry & CIRES, University of Colorado Boulder, 80309 Boulder, CO, USA
[12]California Institute of Technology, Division of Chemistry and Chemical Engineering 210-41, Pasadena, CA 91125, USA
[13]School of Civil and Environmental Engineering, Pusan National University, Busan 46241, Republic of Korea
[14]CERN, 1211 Geneva, Switzerland
[15]P. N. Lebedev Physical Institute of the Russian Academy of Sciences, Laboratory of Solar and Cosmic Ray Physics. 119991 Moscow, Russia
[16]Finnish Meteorological Institute, 00560 Helsinki, Finland
[17]Joint International Research Laboratory of Atmospheric and Earth System Research, School of Atmospheric Sciences, Nanjing University, Nanjing, China.
[18]IDL-Universidade da Beira Interior, 6201-001 Covilhã, Portugal
[19]Aerodyne Research, 01821 Billerica, MA, USA
[a]Now at: Tofwerk AG, 3600 Thun, Switzerland
[b]Now at: Forest Dynamics, Swiss Federal Institute for Forest, Snow and Landscape Research WSL, 8903 Birmensdorf, Switzerland; Department of Chemistry, University of California, 92697 Irvine, CA, USA
Correspondence to: Imad el Haddad (imad.el-haddad@psi.ch), Dongyu Wang (dongyu.wang@psi.ch), Jay G. Slowik (jay.slowik@psi.ch)
* These authors contributed equally to this work

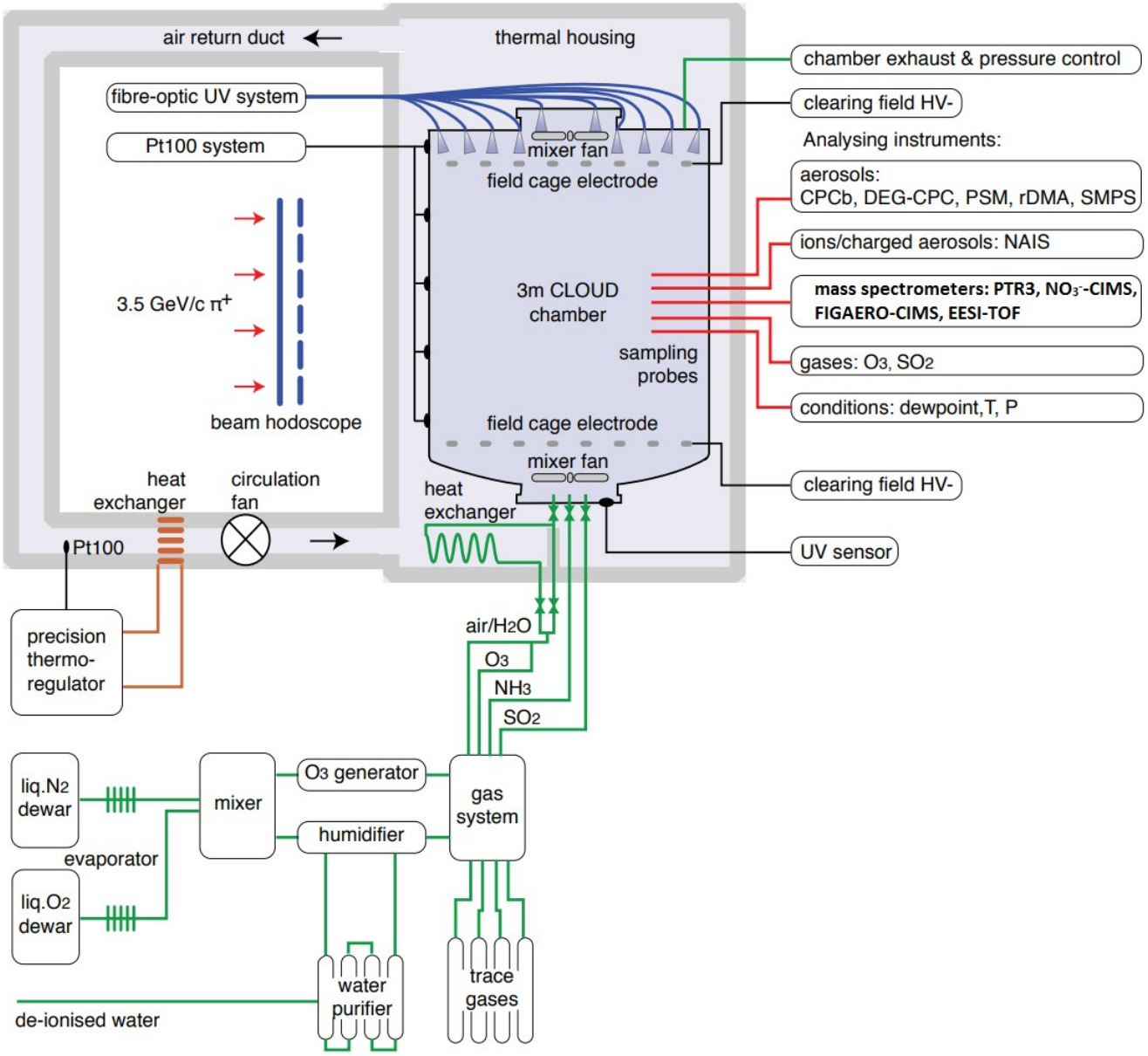

45 **Figure S1**: Schematic of the CLOUD chamber at CERN. Adapted from Kirkby et al. (2011).

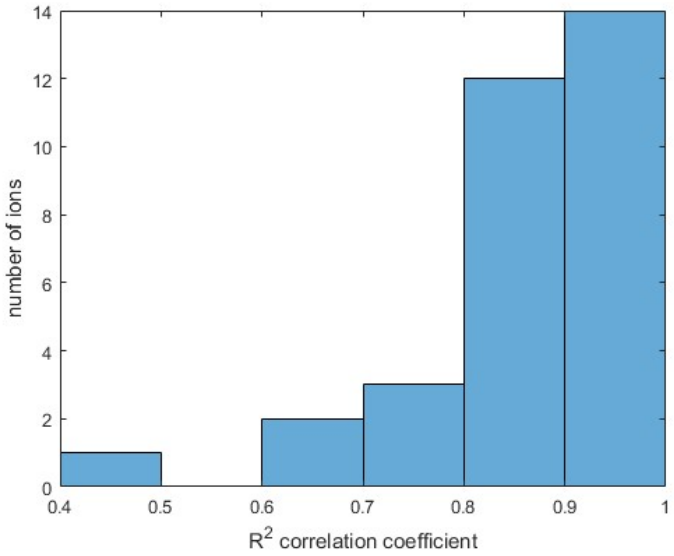

Figure S2. Correlation of the time series of ions identified by both the EESI-TOF and FIGAERO-CIMS for Experiment 1.

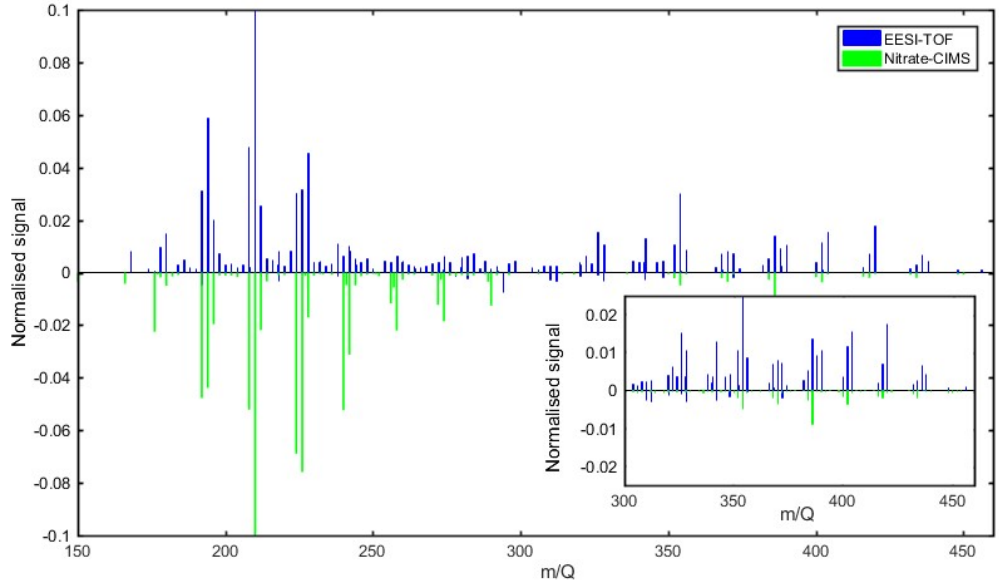

Figure S3: Mass spectra of EESI-TOF (blue) and Nitrate-CIMS (green) naphthalene oxidation products. The spectra are normalized so that the sum of all peaks is equal to one. Dimer region expanded in inset.

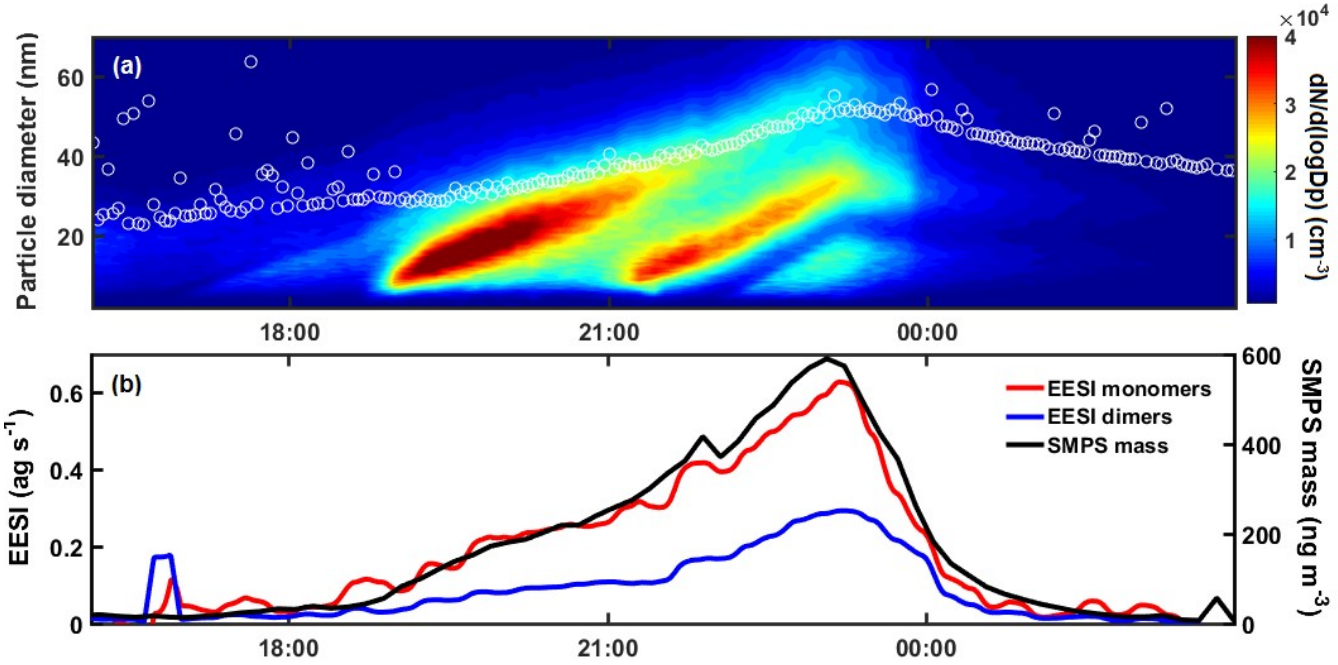

Figure S4. (a) Particle size distribution for a naphthalene experiment without NO_x (Experiment 2) **(b)** Time evolution of the sums of the monomer (sum of C8, C9 and C10 compounds) and dimer (C20) oxidation products from naphthalene measured by the EESI-TOF together with the total mass measured by the SMPS.

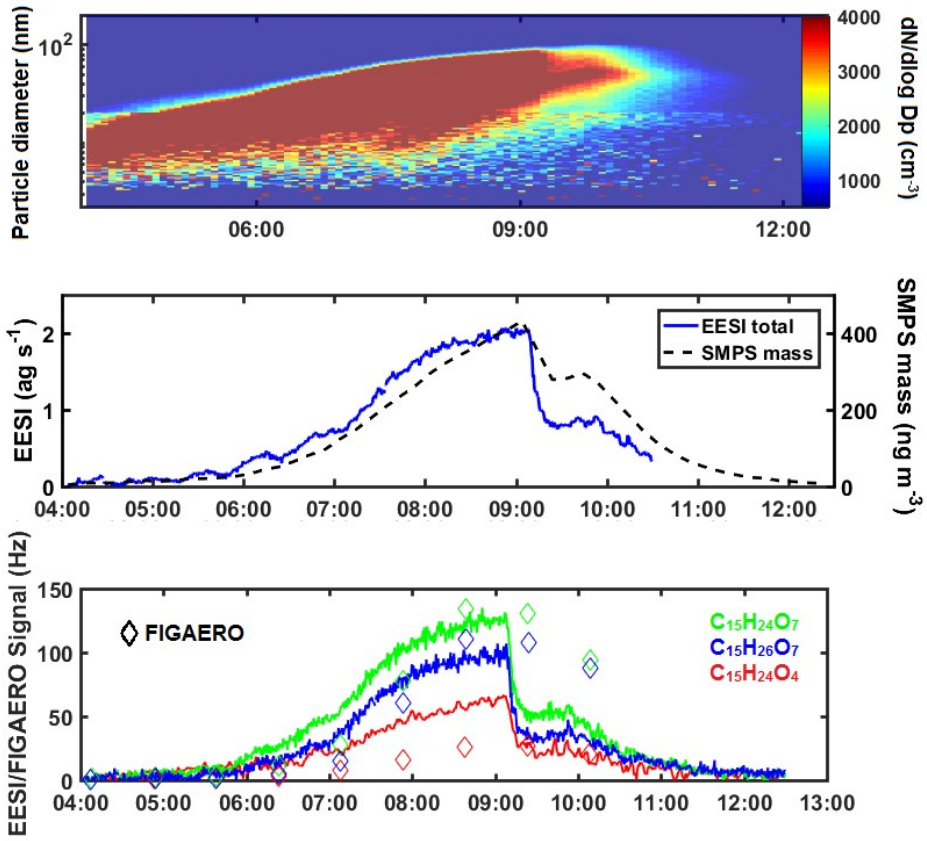

Figure S5. (a) Particle size distribution for a beta-caryophyllene experiment (Experiment 3) **(b)** Total EESI mass and total SMPS mass **(c)**:Time series of selected beta-caryophyllene oxidation products as measured by the EESI-TOF (solid lines) and FIGAERO-CIMS (diamonds).

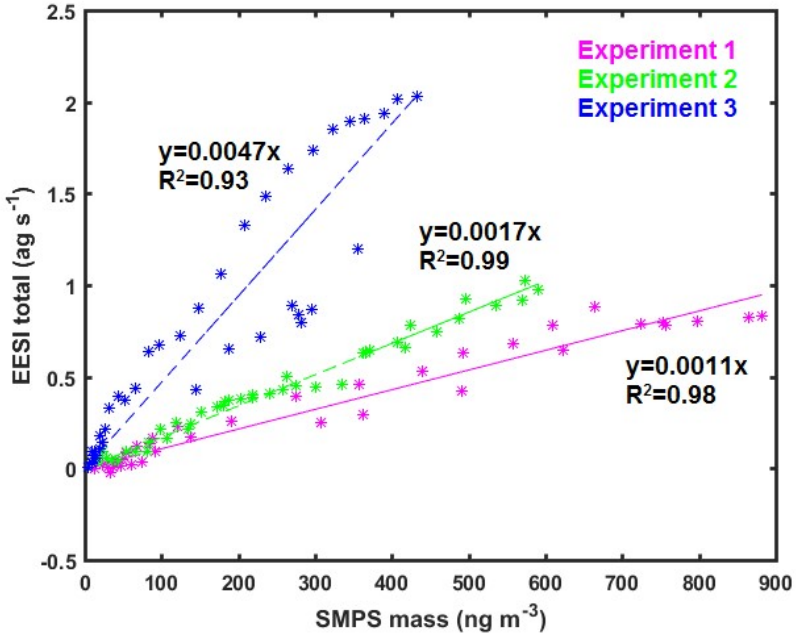

Figure S6: Correlation plot of total EESI mass flux reaching the detector and mass from the SMPS for all the experiments analyzed in this work. The y-intercept of the linear fit is forced to pass through the origin.

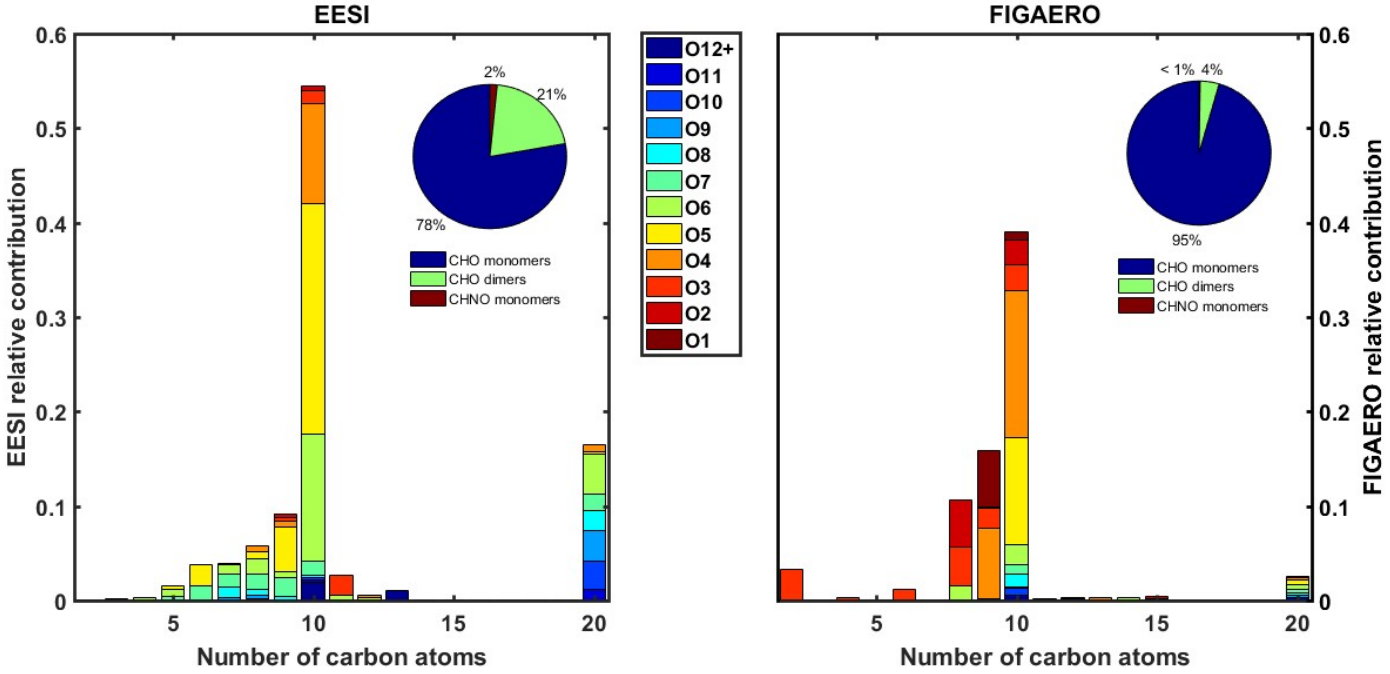

Figure S7. Carbon number distribution for naphthalene SOA in the absence of NO_x (Experiment 2) as detected by the EESI-TOF (left) and FIGAERO-CIMS (right), coloured by number of oxygen. The fractional contributions to the total aerosol signal of nitrogenated and non-nitrogenated monomers and dimers in the FIGAERO-CIMS and EESI-TOF are shown in

insets.

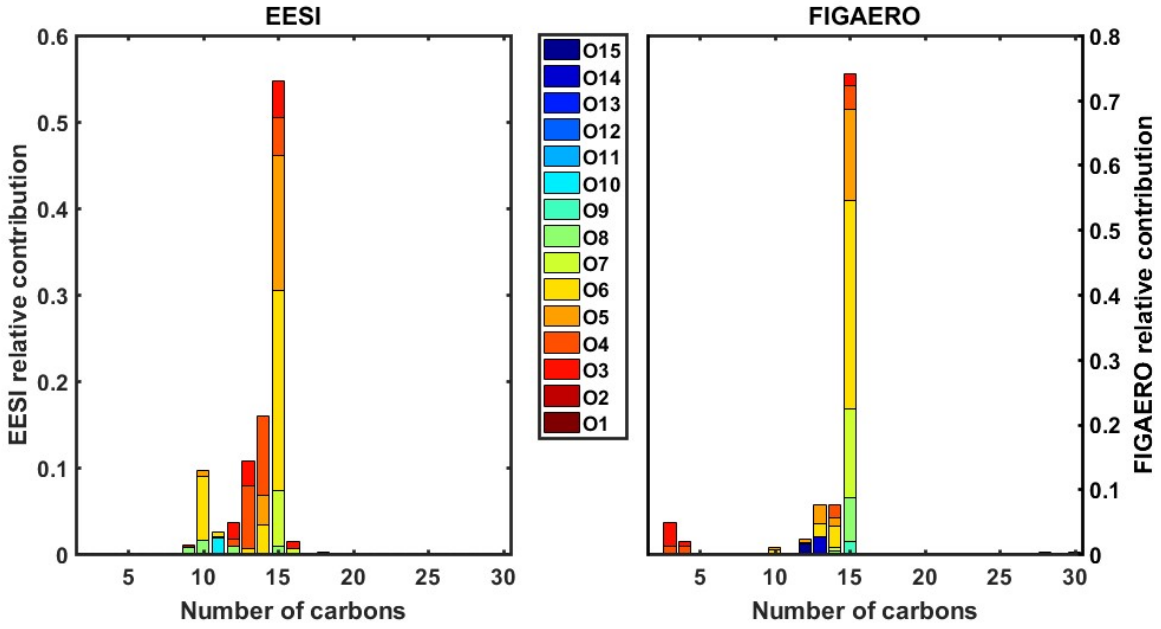

Figure S8. Carbon number distribution for beta-caryophyllene SOA (Experiment 3) as detected by the EESI-TOF (left) and FIGAERO-CIMS (right), coloured by number of oxygen.

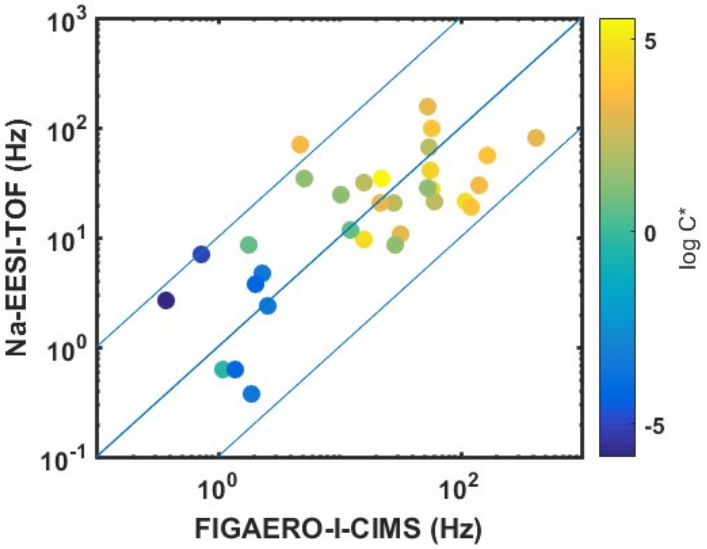

Figure S9: Scatter-plot of signal intensities of naphthalene oxidation products identified by both EESI-TOF and FIGAERO-CIMS for Experiment 1, coloured by volatility. The solid blue lines represent the 10:1, 1:1 and 1:10 ratios.

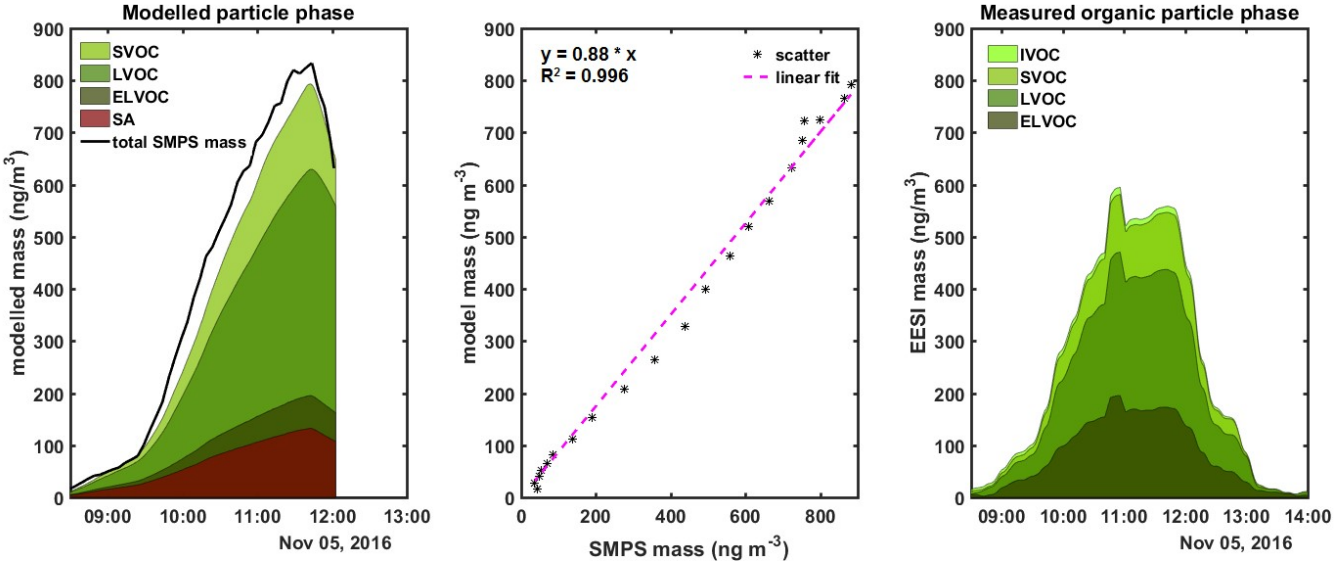

Figure S10. (left) Stacked modelled particle mass (above 6 nm) of total, ELVOC, LVOC, SVOC and sulfate (SA) particle-phase naphthalene oxidation products. The ELVOC bin is an overflow bin and thus contains all compounds with log C^* < -4.5. Total SMPS mass overlaid as solid black line**. (middle)** Correlation plot of total mass from the aerosol growth model and the SMPS. Linear fit line is forced through the origin **(right)** Stacked measured concentrations of total, ELVOC, LVOC, SVOC, IVOC particle-phase naphthalene oxidation products from the EESI- TOF, assuming a uniform response factor, for the entire duration of Experiment 2.

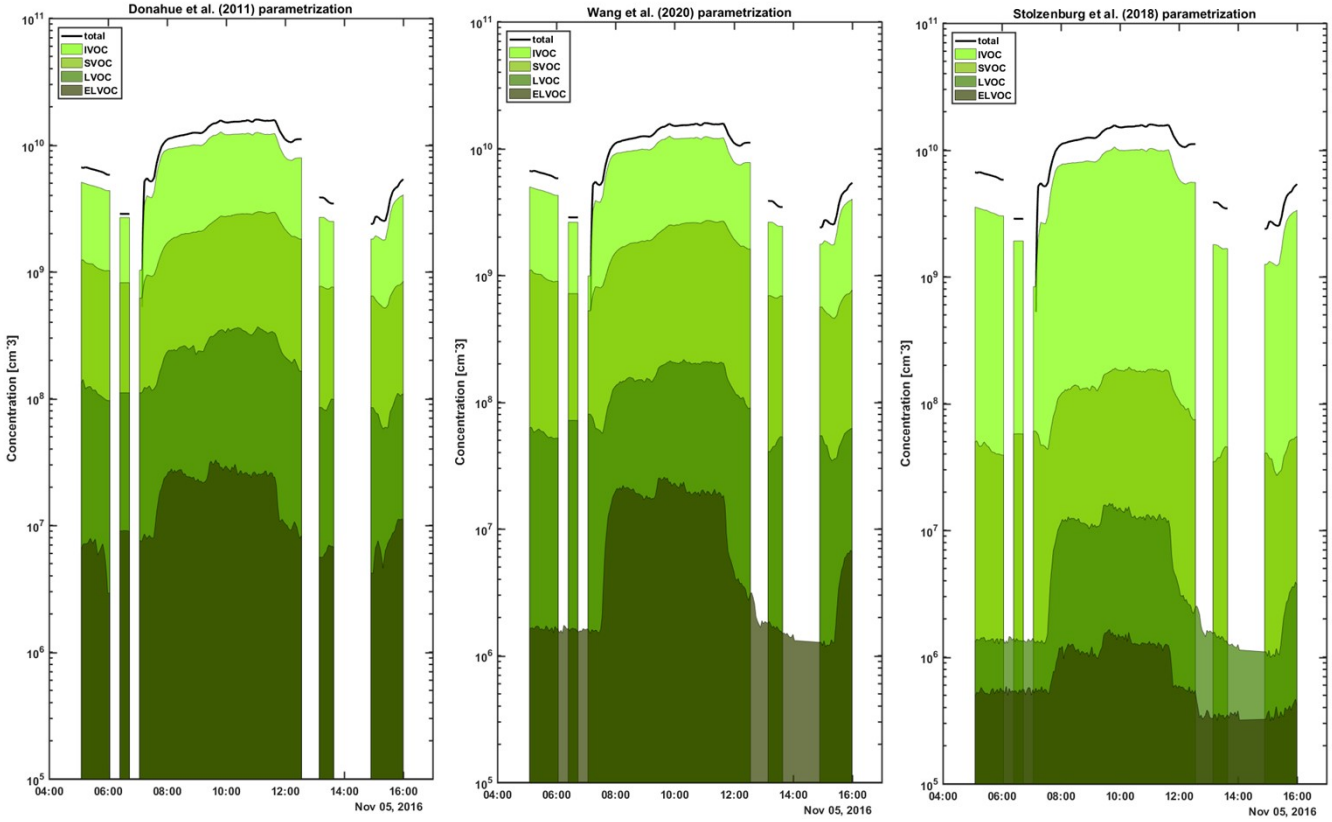

Figure S11. Combined gas phase concentrations measured by the PTR3 and the Nitrate-CIMS, binned according to their estimated volatility provided by different parametrizations: **(left)** Donahue et al., 2011 **(middle)** Wang et al., 2020 **(right)** Stolzenburg et al., 2018.

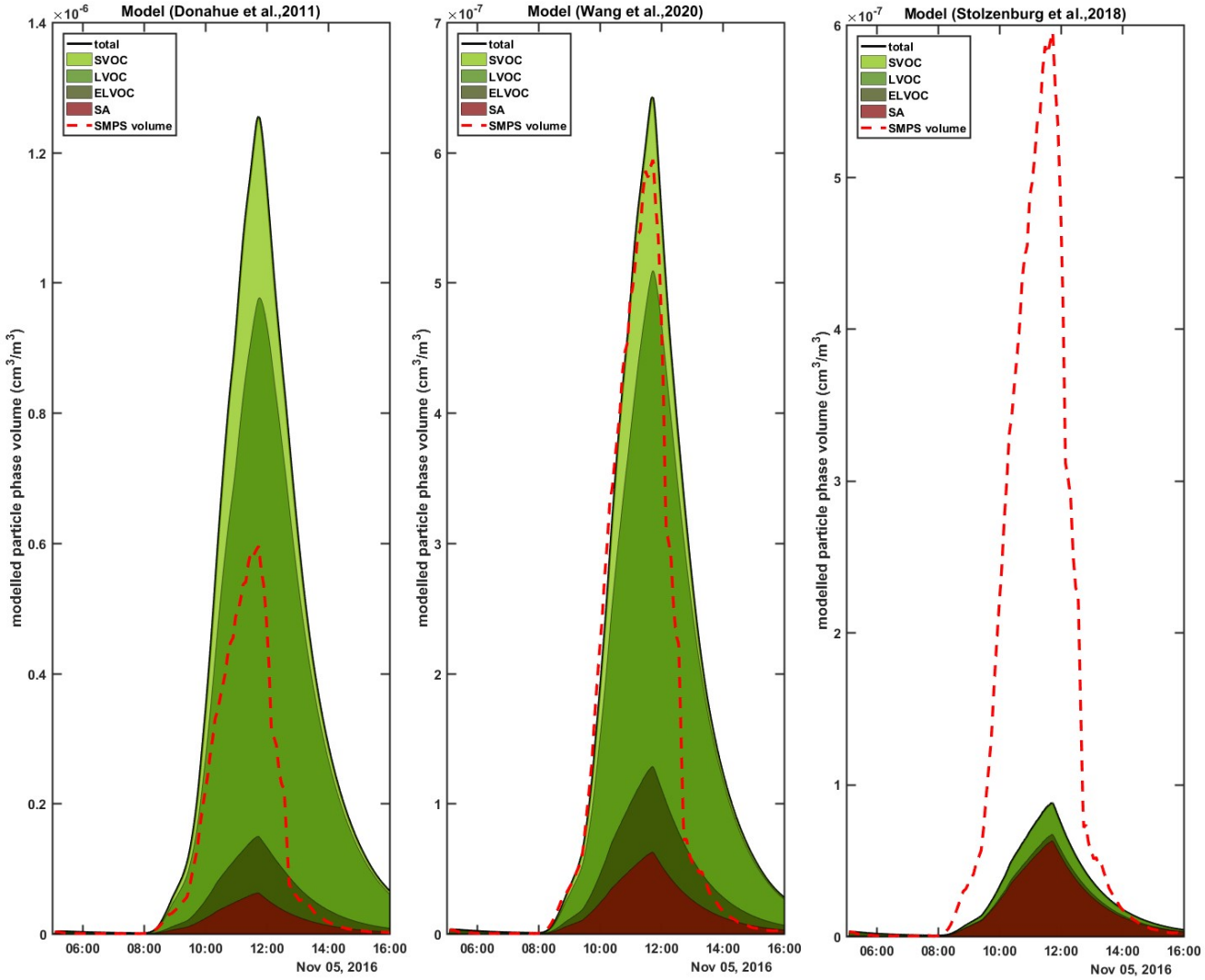

Figure S12. Modelled particle phase according to different parametrizations **(left)** Donahue et al., 2011 **(middle)** Wang et al., 2020 **(right)**. Stolzenburg et al., 2018. Active (HV field + fans) cleaning starting at 12:03 is not considered in the model. Note that the y-axis scale is different between panels a, b and c.

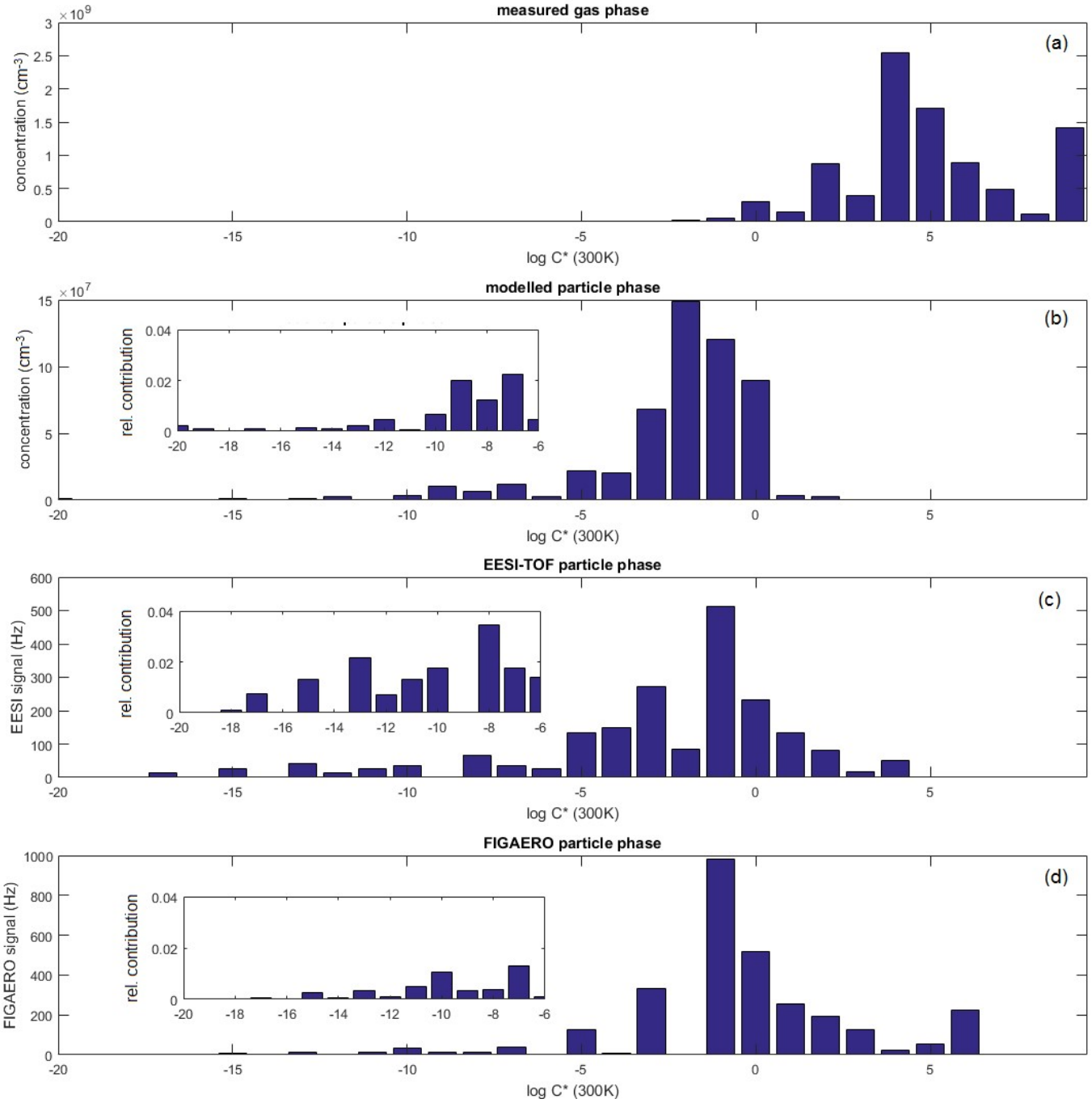

Figure S13. Estimated volatility distributions of naphthalene oxidation products: **(a)** measured gas phase **(b)** modelled particle phase, and **(c)** particle phase measured by the EESI-TOF and **(d)** FIGAERO-CIMS. Relative contributions at maximum mass concentration of bins with log C^* < -6 expanded in inset.

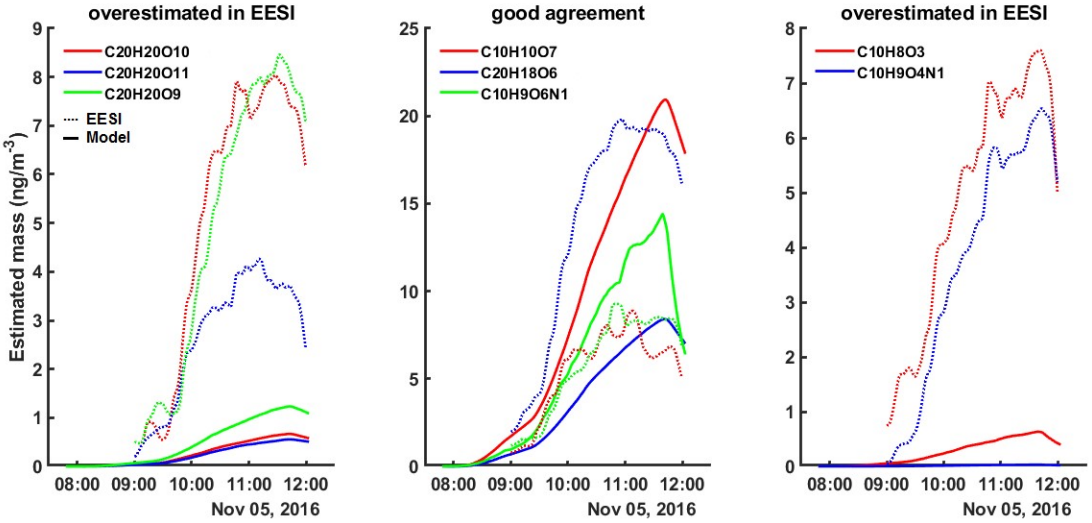

105 **Figure S14.** Example time series of ions overestimated and in good agreement in the EESI-TOF particle-phase data compared to the aerosol growth model results. Dotted lines correspond to measured EESI-TOF data while solid lines are modelled concentrations.

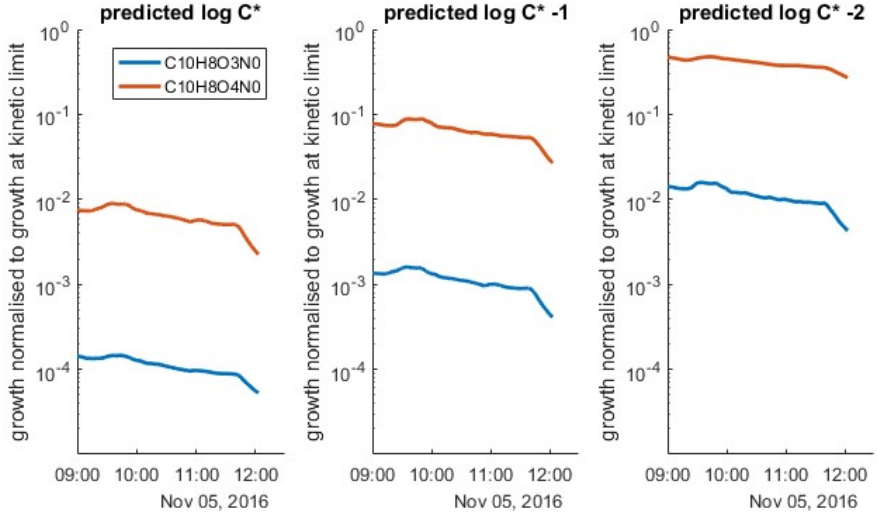

110 **Figure S15.** Example effect of changing the estimated volatility by 1 (middle) and 2 orders of magnitude (right) compared to the predicted one (left) for selected ions that appear more abundant in the EESI-TOF data compared to the aerosol growth model results.

115